Dalton Transactions

ROYAL SOCIETY OF CHEMISTRY

PAPER

View Article Online
View Journal | View Issue

Cite this: *Dalton Trans.*, 2020, **49**, 6661

Luminescent lanthanide complexes with a pyridine-bis(carboxamide)-bithiophene sensitizer showing wavelength-dependent singlet oxygen generation†

Katherine R. Johnson,[a] Sebastian B. Vittardi,[b] Manuel A. Gracia-Nava,[a] Jeffrey J. Rack *[b] and Ana de Bettencourt-Dias *[a]

Received 18th March 2020,
Accepted 29th April 2020

DOI: 10.1039/d0dt01034k

rsc.li/dalton

A new pyridine-bis(carboxamide)-based ligand with a bithiophene pendant, 2Tcbx, was synthesized. Its lanthanide ion (Ln^{III}) complexes, $[Ln(2Tcbx)_2]^{3+}$, were isolated and their photophysical properties were explored. Upon excitation at 360 nm, these complexes display emission in the near-infrared (NIR) with efficiencies of 0.69% for Ln^{III} = Yb^{III}, 0.20% for Ln^{III} = Nd^{III}, and 0.01% for Ln^{III} = Er^{III}, respectively. Concurrent $^1O_2$ formation was seen for all complexes, with efficiencies of 19% for the Yb^{III} complex, 25% for the Nd^{III} complex, and 9% for the Er^{III} complex. When exciting at a longer wavelength, 435 nm, only Ln^{III} emission was observed and larger efficiencies of Ln^{III}-centered emission were obtained. The lack of $^1O_2$ generation indicates that energy pathways involving different ligand conformations, which were investigated by transient absorption spectroscopy, are involved in the sensitization process, and enable the wavelength-dependent generation of $^1O_2$.

Introduction

Lanthanide (Ln^{III}) luminescence, which arises from f–f transitions, is ideal for imaging applications due to the characteristic luminescence spectra for each Ln^{III} ion and the emission colour purity.[1] Because of the forbidden nature of these transitions, the metal-centred emission is efficiently sensitized through coordinated ligands, which results in large Stokes shifts of sensitized emission.[2] The coordinated ligands absorb energy to populate a ligand-based singlet excited state, ^1S. Subsequent intersystem crossing (ISC) generates a ligand-based triplet excited state, ^3T. Energy transfer from the ^3T state to the Ln^{III}-based f* excited state leads to metal-centred luminescence. This sensitization process is referred to as the antenna effect (Fig. 1).[2]

The use of organic ligands as sensitizers allows tailoring the resulting complexes to have dual properties, as was recently reviewed.[3] Examples of Ln^{III} complexes with dual properties include MRI contrast agents that also sense oxygen,[4]

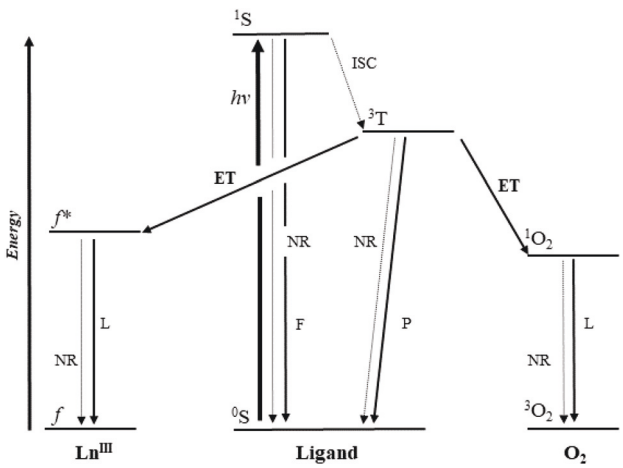

Fig. 1 Energy level diagram showing the energy transfer (ET) pathways for both Ln^{III} ion sensitization and $^1O_2$ generation. Energy $h\nu$ is absorbed by the ligand to populate a singlet excited state (^1S). Intersystem crossing (ISC) leads to the population of a triplet excited state (^3T). This state can then transfer energy to populate the emissive f* excited state which decays by luminescence (L) to the ground state f. Alternatively, the energy transfer leads to $^1O_2$ generation, which decays to triplet oxygen $^3O_2$ by emitting at 1270 nm. Nonradiative (NR) (dash-dot lines) pathways lead to quenching of excited states. Competing radiative processes are fluorescence (F) and phosphorescence (P). Energy levels are not drawn to scale.

[a]*Department of Chemistry, University of Nevada, Reno, Nevada, 89557, USA. E-mail: ad@unr.edu*
[b]*Department of Chemistry and Chemical Biology, University of New Mexico, Albuquerque, NM 87131, USA*

†Electronic supplementary information (ESI) available. CCDC 1990459. For ESI and crystallographic data in CIF or other electronic format see DOI: 10.1039/d0dt01034k

MRI contrast agents that generate singlet oxygen ($^1O_2$),[5] Nd^{III}-doped nanoparticles with chlorin-e6 appended to its surface that generate $^1O_2$ as well and that lead to *in vivo* tumour reduction,[6] porphyrin-based Ln^{III} complexes emitting in the near-infrared (NIR) with efficiencies of $^1O_2$ generation (ϕ_{1O2}) in the range 1.5–4%,[7] and a Tb^{III} complex with appended naphthyl and azaxanthonyl functional groups with Tb^{III}-centred emission efficiency (ϕ^{Tb}) of 24% and ϕ_{1O2} = 12%.[8] Some of us recently reported naphthalimide-based complexes with concurrent emission from visible- and NIR-emitting Ln^{III} ions and $^1O_2$ generation with ϕ_{1O2} up to 64%.[9]

Compounds with the ability to generate $^1O_2$ are useful in therapeutic[10–16] and agricultural applications,[17] among others.[18–20] The toxicity of $^1O_2$ arises from its ability to oxidize biomolecules.[16,21–24] Widely studied $^1O_2$ generators include tetrapyrroles and related molecules,[12,16,20,25] yet their use is limited by their dark toxicity, cutaneous photosensitivity, and dimer formation, which decreases the photosensitizing efficiency.[26] Poor solubility[27] and aggregation[28] shorten the lifetime of the excited state, resulting in low ϕ_{1O2}.[29] Unlike these functional groups, BODIPY dyes do not suffer as strongly from photobleaching, and can be easily synthesized.[14,30,31] Metal–organic frameworks (MOFs) have been successfully used to generate $^1O_2$, leading to the oxidation of alcohols[32] and mustard gas,[33] as well as sensing O_2 in solution.[34] However, ϕ_{1O2} for these systems strongly depends on the nature of the coordinated metal, as it promotes ISC through the heavy atom effect.[35] Fullerenes also generate $^1O_2$ and C_{60} has ϕ_{1O2} of 1; however, surface functionalization to increase solubility disrupts the core, which decreases ϕ_{1O2}.[36] More recently, nanoparticles have been actively pursued as $^1O_2$ generators, despite presenting significant challenges with isolation of pure systems and with long-term stability.[10,13,37,38] Despite the limitations mentioned above, small molecule-based systems are actively pursued due to the ability to tune their properties through further functionalization.

We became interested in thiophene-based ligands, as they display interesting photophysical properties.[39–41] Oligothiophenes, such as 2,2′-bithiophene and 2,2′:5′,2″-terthiophene, are biologically active floral pigments, and are well-studied $^1O_2$ generators with ϕ_{1O2} ranging from 60 to 86%.[42] Our group has recently described a thiophene-based system that generates $^1O_2$ and sensitizes red Eu^{III} emission with ϕ^{Eu} = 25%,[43] as well as oligothiophenes, which are phototoxic and are luminescent in the visible (Eu^{III}) and NIR range (Yb^{III}, Nd^{III}).[44] A limitation of these photosensitizers is that they luminesce and generate $^1O_2$ simultaneously, and upon light exposure will harm cells/tissues in their path. To explore safer alternatives, we have developed dual functional luminescent compounds which generate $^1O_2$ at specific excitation wavelengths. We recently described 3Tcbx, a pyridine-bis(carboxamide) functionalized with terthiophene. Its Ln^{III} complexes demonstrate NIR luminescence and $^1O_2$ generation simultaneously when irradiated at 400 nm. We also reported that when irradiating at lower energy (490 nm) the complexes do not generate $^1O_2$, leading to wavelength-dependent $^1O_2$ generation.[45]

Here, we report the synthesis, characterization, and photophysical properties of a bithienyl-derivatized *N*,*N*,*N*′,*N*′-tetraethyl-pyridine-2,6-dicarboxamide photosensitizer, 2Tcbx, and its luminescent Ln^{III} complexes. In analogy to the 3Tcbx complexes, the 2Tcbx-based complexes show only Ln^{III}-centred emission, or concurrent Ln^{III} emission and $^1O_2$ generation, depending on the excitation wavelength.

Results and discussion

2Tcbx, shown in Fig. 2, was prepared by Pd-catalyzed Suzuki–Miyaura cross-coupling between 4-bromopyridine-2,6-dicarboxamide and the boronic acid of 2,2′-bithiophene (Fig. S1†). It was recovered in 32% yield after purification and was characterized using standard techniques, including single crystal X-ray diffraction (Fig. S2–S8† and Fig. 2).

2Tcbx crystallized in the *Pna*2(1) space group with unit cell parameters of a = 7.67 Å, b = 17.29 Å, c = 17.15 Å, and V = 2273 Å^3. Crystallographic details are summarized in Table S1,† and selected bond distances and angles are available in Table S2 (ESI†). The structure consists of a pyridine ring with bis(carboxamide) functional groups at the 2- and 6-positions as well as a bithiophene moiety at the 4-position. We do observe thiophene-related disorder for the terminal thiophene, which has been reported in other thiophene-containing molecules.[46–48] The centremost thiophene ring is slightly twisted from the plane of the pyridine ring, with a torsion angle (C11–C9–C8–S2) of 27.8(3)°. This angle is similar to what has been reported for 2-thienyl groups, which range from 9.36°–21.0°.[49–53] In addition, the thiophene moieties are slightly twisted from each other, with angles of S2–C5–C4–C3 = 13.54(51)° and S1–C4–C5–C6 = 16.14(38)° for the centremost and terminal thiophene, respectively.

The amide oxygen atoms point in opposite directions and away from the pyridine ring, as observed for other uncoordinated pyridine-bis(carboxamide) compounds.[54,55] They will

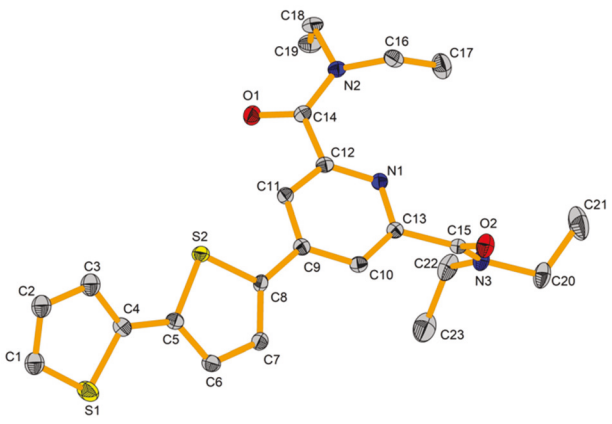

Fig. 2 Thermal ellipsoid plot of 4-aminopyridine-2,6-dicarboxamide. Ellipsoids are shown at the 50% probability level. Hydrogen atoms are omitted for clarity.

Table 1 Singlet (^{1}S) and triplet (^{3}T) excited state energies, quantum yields of fluorescence (ϕ^F), sensitized luminescence (ϕ^{Ln}), and $^1O_2$ generation (ϕ_{1O2}) of nTcbx and its metal complexes ($[Ln(nTcbx)_2]^{3+}$ where Ln^{III} = Gd^{III}, Yb^{III}, Nd^{III}, or Er^{III} and n = 2 or 3) in acetonitrile at 25.0 ± 0.1 °C

			Gd^{III}				Yb^{III}		Nd^{III}		Er^{III}	
	ϕ^F [%]	ϕ_{1O2} [%]	^{1}S [cm^{-1}]	^{3}T [cm^{-1}]	ϕ^F [%]	ϕ_{1O2} [%]	ϕ^{Yb} [%]	ϕ_{1O2} [%]	ϕ^{Nd} [%]	ϕ_{1O2} [%]	ϕ^{Er} [%]	ϕ_{1O2} [%]
2Tcbx, λ_{exc} = 360 nm	56 ± 2	29 ± 3	25 000 ± 60	23 500 ± 70	62 ± 4	37 ± 4	0.08 ± 0.01	19 ± 3	0.09 ± 0.03	25 ± 3	0.01 ± 0.00	9 ± 1
2Tcbx, λ_{exc} = 435 nm	*b*	*b*			*b*	*b*	0.69 ± 0.04	*b*	0.20 ± 0.04	*b*	0.02 ± 0.01	*b*
3Tcbx,[c] λ_{exc} = 400 nm	9 ± 1	60 ± 6	22 700 ± 70	21 300 ± 10	13 ± 2	62 ± 1	0.02 ± 0.01	11 ± 1	0.05 ± 0.00	11 ± 3	*a*	13 ± 3
3Tcbx,[c] λ_{exc} = 490 nm	*b*	*b*			*b*	*b*	0.29 ± 0.03	*b*	0.16 ± 0.04	*b*	*a*	*b*

[a] Emission was not quantifiable. [b] Emission was not observed. [c] Work from ref. 45.

point in the same direction of the pyridine nitrogen atom, once coordinated to a Ln^{III} ion.

In acetonitrile, 2Tcbx shows an absorption maximum at 360 nm (Fig. S9†) with a molar absorptivity (ε) of ~36 000 M^{-1} cm^{-1}. It emits in the visible region of the spectrum with a maximum at 435 nm (Fig. S10†) and a fluorescence quantum yield (ϕ^F) of 56% (Table 1). These values are similar to other oligothienyl-based systems where ϕ^F range from 2 to 65%.[45,56,57] 2Tcbx is a $^1O_2$ generator in acetonitrile as evidenced by the emission peak at 1270 nm (Fig. S11†), with ϕ_{1O2} of 29%. This value is comparable to other aryl-substituted oligothiophenes, with reported ϕ_{1O2} ranging from 2 to 80%,[42,44,45,58,59] and is less efficient at $^1O_2$ generation than 3Tcbx (ϕ_{1O2} = 60%).[45] Excitation at 435 nm did not lead to $^1O_2$ generation or ligand fluorescence (*vide infra*).

Ln^{III} ion complexes were isolated by mixing 2Tcbx with $Ln(NO_3)_3$ (Ln = Nd^{III}, Gd^{III}, Er^{III}, and Yb^{III}) in acetonitrile (Fig. S12, S13 and Table S3†). The speciation diagrams (Fig. S12b and S13b†) show that solutions with the 2 : 1 species, $[Ln(2Tcbx)_2]^{3+}$, as the dominant species can be prepared, in analogy to what was observed for the 3Tcbx-based system.[45] This stoichiometry was therefore used for photophysical characterization.

All metal complexes were prepared by mixing one equivalent of $Ln(NO_3)_3$ (Ln^{III} = Eu^{III}, Gd^{III}, Yb^{III}, Nd^{III}, or Er^{III}) with 2 equivalents of 2Tcbx. Once combined, the mixtures were refluxed in acetonitrile and the solvent removed under reduced pressure (see ESI†). Their formation was confirmed by high-resolution mass spectrometry (Fig. S5–S8†). For spectroscopic studies the complexes were generated in solution and not isolated.

To assess the ability of 2Tcbx to act as sensitizer of Ln^{III} luminescence, the ^{1}S and ^{3}T energies of the Gd^{III} complex[60] were determined in degassed n-hexanes and are at 25 000 and 23 500 cm^{-1} (Fig. S14 and S15†), respectively. These are high enough to sensitize Nd^{III}, Yb^{III}, and Er^{III} luminescence. Although the ^{3}T state appears high enough to sensitize Eu^{III}, a visible emitter, only very weak Eu^{III} emission was observed, and therefore this complex was not further pursued for this study.

Upon excitation at the absorption maximum, the characteristic metal-centred emission is observed. For $[Yb(2Tcbx)_2]^{3+}$, the spectrum displayed the typical transition $^2F_{5/2} \rightarrow {}^2F_{7/2}$ at 976 nm. For $[Nd(2Tcbx)_2]^{3+}$ the $^4F_{3/2} \rightarrow {}^4I_J$ (J = 9/2–13/2) transitions with a maximum at 1053 nm are observed. The $^4I_{13/2} \rightarrow {}^4I_{15/2}$ transition at 1513 nm for $[Er(2Tcbx)_2]^{3+}$ was also observed. Quantum yields of sensitized Ln^{III} emission (ϕ^{Ln}) for these complexes are summarized in Table 1. $[Yb(2Tcbx)_2]^{3+}$ has ϕ^{Yb} = 0.08%, $[Nd(2Tcbx)_2]^{3+}$ has ϕ^{Nd} = 0.09%, and $[Er(2Tcbx)_2]^{3+}$ has ϕ^{Er} = 0.01% (Table 1). These values are comparable to other Yb^{III}, Nd^{III} and Er^{III} complexes,[43,45,61–66] and are notably higher than what is observed for the 3Tcbx-based systems (Table 1).[45]

In addition to sensitizing Ln^{III} emission, these complexes generate $^1O_2$ when excited at 360 nm, as evidenced by the emission peak at 1270 nm (Fig. 3). ϕ_{1O2} are 19% for $[Yb(2Tcbx)_2]^{3+}$, 25% for $[Nd(2Tcbx)_2]^{3+}$, and 9% for $[Er(2Tcbx)_2]^{3+}$ (Table 1). The largest ϕ_{1O2} value of 37% was obtained for $[Gd(2Tcbx)_2]^{3+}$, indicating that by coordinating luminescent Ln^{III} ions (Nd^{III}, Yb^{III} or Er^{III}) to 2Tcbx, ϕ_{1O2} decreases due to the competing Ln^{III} luminescence.

Additional photophysical characterization of these compounds revealed that, in analogy to what was observed for 3Tcbx,[45] the maxima of the excitation spectra obtained when monitoring the Ln^{III} emission (Nd^{III} at 1053 nm, Yb^{III} at 980 nm, and Er^{III} at 1513 nm) are red-shifted by ~45 nm when

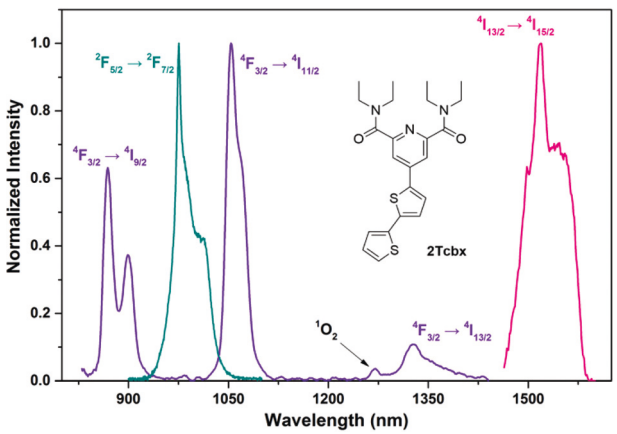

Fig. 3 Emission spectra of $[Ln(2Tcbx)_2]^{3+}$ in acetonitrile at 25.0 ± 0.1 °C (Ln = Nd^{III} (purple), Yb^{III} (teal), Er^{III} (pink)). $^1O_2$ emission at 1270 nm is shown for Nd^{III} only, for clarity, but is observed for all three complexes. The 2Tcbx molecule is pictured.

compared to the excitation spectra obtained when monitoring the $^1O_2 \rightarrow {}^3O_2$ transition at 1270 nm (Fig. S16†). As observed for 3Tcbx, when measuring the emission spectra of all luminescent compounds using a lower energy excitation wavelength, we did not observe $^1O_2$ emission. For example, when $[Er(2Tcbx)_2]^{3+}$ is excited at 360 nm, we observed both Er^{III} luminescence and $^1O_2$ phosphorescence (Fig. 4, black trace); however, when $[Er(2Tcbx)_2]^{3+}$ is excited at 435 nm, we observed only Er^{III} emission (Fig. 4, blue trace). This is similar to what is observed for the 3Tcbx-based complexes,[45] but in this case, a different energy transfer mechanism is in operation.

ϕ^{Ln} were also determined at 435 nm excitation for $[Ln(2Tcbx)_2]^{3+}$ and are summarized in Table 1. $[Yb(2Tcbx)_2]^{3+}$ has a $\phi^{Yb} = 0.69\%$, which is higher than the efficiencies at shorter wavelengths (0.08%). This higher value is similar to what is reported for known Yb^{III} complexes.[61–66] A similar increase in emission efficiency is observed for the Nd^{III} complex, where $\phi^{Nd} = 0.20\%$ is higher than the 0.09% obtained at shorter excitation wavelengths. This higher value is comparable to other known Nd^{III} complexes.[61–66] $[Er(2Tcbx)_2]^{3+}$ has a $\phi^{Er} = 0.02\%$, which is again comparable to known complexes. 3Tcbx sensitizes only weakly Er^{III}-centred emission.[45]

The ability of 2Tcbx to sensitize Ln^{III} luminescence is, in all cases, higher than what was observed for 3Tcbx. For example, ϕ^{Nd} of $[Nd(3Tcbx)_2]^{3+}$ was 0.05% while $^1O_2$ is simultaneously generated and 0.16% when $^1O_2$ is not formed. ϕ^{Nd} of $[Nd(2Tcbx)_2]^{3+}$ is 0.09% while generating $^1O_2$ simultaneously and 0.20% when $^1O_2$ is not formed. This trend is also observed when comparing the Yb^{III} complexes, as shown in Table 1.

For all complexes, we verified that there is no detectable $^1O_2$ emission at 1270 nm at the longer excitation wavelength. This is consistent with the observed increase in ϕ^{Ln} when $^1O_2$ is not generated; because energy transfer occurs through the triplet excited state, sensitization of metal-centred luminescence and molecular O_2 are competitive processes.

While both the 2Tcbx- and 3Tcbx-based systems show the wavelength-dependent generation of $^1O_2$, there are some notable differences, as discussed below.

We expect that the additional thiophene ring for 3Tcbx relative to 2Tcbx results in a smaller HOMO–LUMO energy gap, as is observed for 2,2′-bithiophene and 2,2′:5′,2″ terthiophene, which are at 8.3 and 9.3 eV, respectively.[67] As such, Ln^{III} emission or concurrent Ln^{III} emission and $^1O_2$ generation in the complexes with 2Tcbx are excited at higher energies, namely 435 nm and 360 nm, and the complexes with 3Tcbx are excited at 490 and 400 nm, respectively.[45]

$^1O_2$ generation efficiencies for $[Yb(2Tcbx)_2]^{3+}$ and $[Yb(2Tcbx)_2]^{3+}$ are higher than those of their 3Tcbx analogues, and similar what is observed for 2,2′-bithiophene ($\phi_{1O2} = 0.98$) and 2,2′:5′,2″-terthiophene ($\phi_{1O2} = 0.74$).[68] However, ϕ_{1O2} is lower for $[Er(2Tcbx)_2]^{3+}$ than for $[Er(3Tcbx)_2]^{3+}$. This is likely due to weak sensitization of Er^{III} luminescence with the 3Tcbx ligand, and therefore, more energy is transferred from the triplet state to generate $^1O_2$.

To understand the unusual photophysical behaviour of these complexes, we investigated the possibility of multiple ligand-based excited states by ultrafast transient absorption spectroscopy. We focused on $[Nd(2Tcbx)_2]^{3+}$ as a representative species in this class, though we also investigated $[Ln(2Tcbx)_2]^{3+}$, where $Ln^{III} = Yb^{III}$, Er^{III}, or Gd^{III} (Fig. S18†). Shown in Fig. 5 are the transient spectra of $[Nd(2Tcbx)_2]^{3+}$ collected with 360 nm (top) and 420 nm (bottom) at different pump–probe time delays. There is a strong similarity of these spectra relative to that obtained for the free, unbound 2Tcbx ligand (Fig. S19†). The initial trace (0.6 ps) features a sharp, narrow excited state absorption (esa) near 540 nm, an intense bleach feature at ~450 nm, and a shallow bleach near 360 nm. The bleach at ~360 nm corresponds well with the ground state absorption (dash-dotted spectrum, Fig. 4, top), but is less intense than expected. The shallow bleach at 450 nm does not correspond to a ground state absorption, but instead appears correlated with emission from $[Nd(2Tcbx)_2]^{3+}$, and thus this feature is assigned to stimulated emission from the complex. We suspect that this stimulated emission overlaps with the ground state absorption, rendering the ground state bleach at 370 nm less intense. As the spectra evolve in time, the narrow excited state absorption near 550 nm shifts slightly blue and decreases in intensity. Concomitant with this change is the emergence of an isosbestic point at 490 nm, loss of the stimulated emission peak and the appearance of a broad excited state absorption at 420 nm. The 7000 ps transient spectrum shows both the esa at 420 nm and a ground state bleach at 360 nm, indicating the formation of a long-lived excited state species that persists onto the nanosecond timescale. Based on the breadth of the esa peak, we ascribe this long-lived species to a triplet state. Again, these spectral changes are strongly reminiscent of what is observed for the free 2Tcbx ligand.

Excitation of $[Nd(2Tcbx)_2]^{3+}$ with 420 nm yields spectral features that broadly consistent with that of the ligand as well as

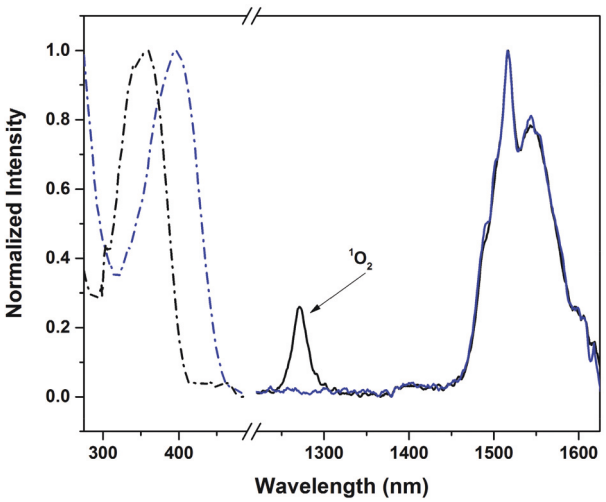

Fig. 4 Excitation (dot-dashed) and emission (solid) spectra of $[Er(2Tcbx)_2]^{3+}$ in acetonitrile at 25.0 ± 0.1 °C. Excitation spectra were collected at 1513 nm (blue) and 1270 nm (black) and emission spectra were collected with excitation wavelengths of 360 (black) and 435 nm (blue).

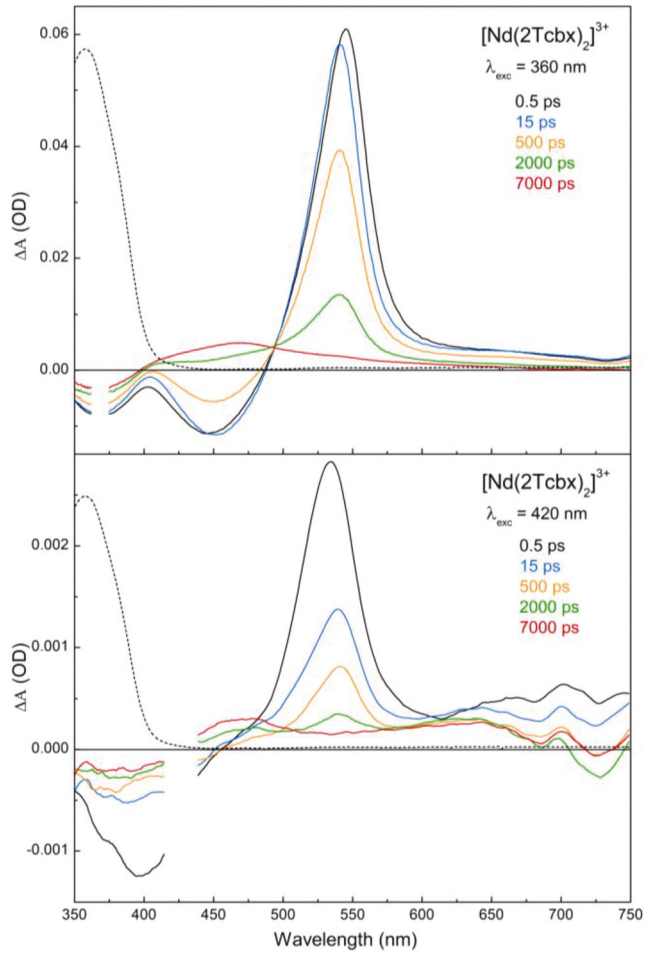

Fig. 5 (Top) Transient spectra of $[Nd(2Tcbx)_2]^{3+}$ collected with 360 nm excitation with different pump probe time delays. Inset legend assigns time delay with coloured trace. (Bottom) Transient spectra of $[Nd(2Tcbx)_2]^{3+}$ collected with 420 nm excitation with different pump probe time delays. Inset legend assigns time delay with coloured trace. The ground state spectrum of $[Nd(2Tcbx)_2]^{3+}$ is represented by the dashed trace in both plots.

the complex with 360 nm excitation, with one exception. For these data, the stimulated emission peak is much less evident even in the sub-picosecond data. While the 420 nm excitation transient data feature a well-defined stimulated emission peak, the 360 nm excitation data never yield a well-defined peak, though one suspects some evidence of emission in the 0.8 ps spectrum. A comparison of the 7000 ps transient spectra in both sets of data shows that these are essentially identical, indicating the same state is formed at this time. The 420 nm excitation transient data are consistent with the emission data from 435 nm excitation discussed above (Fig. 4). We propose that the absence of stimulated emission following 420 nm excitation on the sub-nanosecond timescale provides evidence for distinct photochemistry, since both excitation wavelengths appear to yield the same excited state.

Kinetic analysis from both sets of data in Fig. 5 retrieves a tri-exponential fit with $\tau_1 = 0.95 \pm 0.07$ ps, $\tau_2 = 288 \pm 63$ ps, and $\tau_3 = 1285 \pm 25$ ps for the data collected with 360 nm excitation. In comparison to the 420 nm excitation data, the lifetimes are $\tau_1 = 1.5 \pm 0.2$ ps, $\tau_2 = 106 \pm 44$ ps, and $\tau_3 = 1369 \pm 150$ ps. We also collected and fit the transient data for the free, unbound 2Tcbx ligand. That analysis yielded the following lifetimes, $\tau_1 = 1.0 \pm 0.2$ ps, $\tau_2 = 44 \pm 1$ ps, and $\tau_3 = 1451 \pm 80$ ps. Previous studies on 2,2′-bithiophene similarly yield a triexponential fit of $\tau_1 = 1.1 \pm 0.1$ ps, $\tau_2 = 12 \pm 13.8$ ps, and $\tau_3 > 400$ ps.[69] In agreement with other studies, τ_1 is assigned to relaxation within S_1 from the Franck–Condon state, τ_2 is ascribed to intersystem crossing (ISC) to the triplet states T_2 and T_3, and τ_3 is assigned to relaxation to ground state (S_0).[69–71] Computational data indicate that T_3 is 0.58 eV above S_1, that T_2 is essentially isoenergetic with S_1, and that T_1 is 1.94 eV downhill from S_1.[35,36] However, low energy torsional barriers (<25 meV) for different *syn* and *anti* conformers complicate the dynamics of 2,2′-bithiophene.[72,73] With this in mind, for $[Nd(2Tcbx)_2]^{3+}$, we assign τ_1 to relaxation within S_1 from the Franck–Condon state and τ_2 to ISC to form the T_2. Since either excitation wavelength yields a transient that is longer lived that our instrumental constraints, the longest time constant cannot be ascribed to relaxation to ground state concomitant with energy transfer to Nd^{III}. In that case, one would expect to see loss of all optical density in the pump–probe experiment, and thus a transient that was indistinguishable from the zero line indicating no net photochemistry on that time scale (7 ns). The presence of a long-lived transient indicates that a new state is formed. Our present data does not permit us to make a rigorous assignment here. This new state could be a triplet on the pyridine portion of 2Tcbx. However, we more strongly suspect that this new triplet state is localized on the bithiophene (2T) unit and is in a conformation stabilized by the presence of the Ln^{III} ion. Such an assignment is consistent with our previous study on closely related complexes.[45] We ascribe the difference in photophysical behaviour following 360 nm *vs.* 420 nm excitation to a conformation formed from 360 nm excitation that permits reaction with $^3O_2$ that is not accessible with 420 nm excitation. Alternately, 420 nm excitation yields a conformation that promotes energy transfer to the Nd^{III} and thus no stimulated emission is observed. This is consistent with a higher quantum yield for Nd^{III} emission at longer wavelengths.

It is important to note that this proposed mechanism (see TOC figure) is different from that suggested for the closely related 3Tcbx complexes. For the 3Tcbx complexes, different excitation wavelengths yielded strikingly different electronic excited states, and we deduced that these distinct excited states reacted differentially with $^3O_2$.[45] In the 2Tcbx complexes described above, we have no evidence for the formation of different excited states, thus we propose that different conformations of the same electronic excited state must produce the differential reactivity with $^3O_2$. We find it surprising that the same wavelength dependence for $^1O_2$ production for these closely related complexes ($[Ln(3Tcbx)_2]^{3+}$ *vs.* $[Ln(3Tcbx)_2]^{3+}$) has two different explanations based on femtosecond transient absorption spectroscopy.

Conclusions

We have isolated a new ligand based on bithiophene-derivatized pyridine-bis(carboxamide). We have shown its ability to coordinate Ln^{III} ions and sensitize their emission and to generate $^1O_2$. Because $^1O_2$ generation is wavelength-dependent, these compounds provide the tracking ability of luminescence without sacrificing healthy cells, and would therefore be safer alternatives for therapy and diagnosis. However, these complexes are not water-soluble and thus not useful for bioimaging and therapy purposes. Nonetheless, they provide a roadmap for the development of complexes with wavelength-dependent dual functionality.

Conflicts of interest

The authors declare no conflicts of interest.

Acknowledgements

The National Science Foundation (CHE 1800392 to AdBD and CHE 1856492 to JJR) is gratefully acknowledged for financial support. Prof. Jorge H. S. K. Monteiro (Humboldt State University) is thanked for his assistance with absorption titrations and some emission spectroscopy.

References

1 J. H. S. K. Monteiro, D. Machado, L. M. de Hollanda, M. Lancellotti, F. A. Sigoli and A. de Bettencourt-Dias, *Chem. Commun.*, 2017, **53**, 11818–11821.
2 A. de Bettencourt-Dias, Introduction to Lanthanide Ion Luminescence, in *Luminescence of Lanthanide Ions in Coordination Compounds and Nanomaterials*, ed. A. de Bettencourt-Dias, John Wiley & Sons, Ltd., Chichester, United Kingdom, 2014, pp. 1–48.
3 R. D. Teo, J. Termini and H. B. Gray, *J. Med. Chem.*, 2016, **59**, 6012–6024.
4 A. Jana, B. J. Crowston, J. R. Shewring, L. K. McKenzie, H. E. Bryant, S. W. Botchway, A. D. Ward, A. J. Amoroso, E. Baggaley and M. D. Ward, *Inorg. Chem.*, 2016, **55**, 5623–5633.
5 A. Sour, S. Jenni, A. Orti-Suarez, J. Schmitt, V. Heitz, F. Bolze, P. Loureiro de Sousa, C. Po, C. S. Bonnet, A. Pallier, E. Toth and B. Ventura, *Inorg. Chem.*, 2016, **55**, 4545–4554.
6 X. Ai, C. J. H. Ho, J. Aw, A. B. E. Attia, J. Mu, Y. Wang, X. Wang, Y. Wang, X. Liu, H. Chen, M. Gao, X. Chen, E. K. L. Yeow, G. Liu, M. Olivo and B. Xing, *Nat. Commun.*, 2016, **7**, 10432.
7 T. Lv and W. Sun, *J. Inorg. Organomet. Polym. Mater.*, 2013, **23**, 200–205.
8 G.-L. Law, R. Pal, L. O. Palsson, D. Parker and K.-L. Wong, *Chem. Commun.*, 2009, 7321–7323.
9 K. R. Johnson and A. de Bettencourt Dias, *Inorg. Chem.*, 2019, **58**, 13471–13480.
10 Y. Li, T.-Y. Lin, Y. Luo, Q. Liu, W. Xiao, W. Guo, D. Lac, H. Zhang, C. Feng, S. Wachsmann-Hogiu, J. H. Walton, S. R. Cherry, D. J. Rowland, D. Kukis, C. Pan and K. S. Lam, *Nat. Commun.*, 2014, **5**, 4712.
11 M. E. Davis, Z. Chen and D. M. Shin, *Nat. Rev. Drug Discovery*, 2008, **7**, 771.
12 R. Bonnett, *Chem. Soc. Rev.*, 1995, **24**, 19–33.
13 B. Liu, C. Li, P. Yang, Z. Hou and J. Lin, *Adv. Mater.*, 2017, **29**, 1605434.
14 A. Kamkaew, S. H. Lim, H. B. Lee, L. V. Kiew, L. Y. Chung and K. Burgess, *Chem. Soc. Rev.*, 2013, **42**, 77–88.
15 K. C. Nicolaou, J. S. Chen, D. J. Edmonds and A. A. Estrada, *Angew. Chem., Int. Ed.*, 2009, **48**, 660–719.
16 Z. Malik, J. Hanania and Y. Nitzan, *J. Photochem. Photobiol., B*, 1990, **5**, 281–293.
17 R. J. Marles, R. L. Compadre, C. M. Compadre, C. Soucy-Breau, R. W. Redmond, F. Duval, B. Mehta, P. Morand, J. C. Scaiano and J. T. Arnason, *Pestic. Biochem. Physiol.*, 1991, **41**, 89–100.
18 R. T. Gephart, P. N. Coneski and J. H. Wynne, *ACS Appl. Mater. Interfaces*, 2013, **5**, 10191–10200.
19 Z. Amara, J. F. B. Bellamy, R. Horvath, S. J. Miller, A. Beeby, A. Burgard, K. Rossen, M. Poliakoff and M. W. George, *Nat. Chem.*, 2015, **7**, 489.
20 M. C. DeRosa and R. J. Crutchley, *Coord. Chem. Rev.*, 2002, **233–234**, 351–371.
21 I. O. L. Bacellar, T. M. Tsubone, C. Pavani and M. S. Baptista, *Int. J. Mol. Sci.*, 2015, **16**, 20523–20559.
22 S. Luo, X. Tan, S. Fang, Y. Wang, T. Liu, X. Wang, Y. Yuan, H. Sun, Q. Qi and C. Shi, *Adv. Funct. Mater.*, 2016, **26**, 2826–2835.
23 C. Laloi and M. Havaux, *Front. Plant Sci.*, 2015, **6**, 39.
24 T. Toerring, S. Helmig, P. R. Ogilby and K. V. Gothelf, *Acc. Chem. Res.*, 2014, **47**, 1799–1806.
25 A. De Rosa, D. Naviglio and A. Di Luccia, *Curr. Cancer Ther. Rev.*, 2011, **7**, 234–247.
26 A. E. O'Connor, W. M. Gallagher and A. T. Byrne, *Photochem. Photobiol.*, 2009, **85**, 1053–1074.
27 F. Dumoulin, M. Durmuş, V. Ahsen and T. Nyokong, *Coord. Chem. Rev.*, 2010, **254**, 2792–2847.
28 X.-J. Jiang, P.-C. Lo, Y.-M. Tsang, S.-L. Yeung, W.-P. Fong and D. K. P. Ng, *Chem. – Eur. J.*, 2010, **16**, 4777–4783.
29 P.-C. Lo, J.-D. Huang, D. Y. Y. Cheng, E. Y. M. Chan, W.-P. Fong, W.-H. Ko and D. K. P. Ng, *Chem. – Eur. J.*, 2004, **10**, 4831–4838.
30 S. Atilgan, Z. Ekmekci, A. L. Dogan, D. Guc and E. U. Akkaya, *Chem. Commun.*, 2006, 4398–4400.
31 Y. Yang, Q. Guo, H. Chen, Z. Zhou, Z. Guo and Z. Shen, *Chem. Commun.*, 2013, **49**, 3940–3942.
32 Y.-Z. Chen, Z. U. Wang, H. Wang, J. Lu, S.-H. Yu and H.-L. Jiang, *J. Am. Chem. Soc.*, 2017, **139**, 2035–2044.
33 M. Cao, R. Pang, Q.-Y. Wang, Z. Han, Z.-Y. Wang, X.-Y. Dong, S.-F. Li, S.-Q. Zang and T. C. W. Mak, *J. Am. Chem. Soc.*, 2019, **141**, 14505–14509.

34 R.-W. Huang, Y.-S. Wei, X.-Y. Dong, X.-H. Wu, C.-X. Du, S.-Q. Zang and T. C. W. Mak, *Nat. Chem.*, 2017, **9**, 689–697.
35 L. B. Josefsen and R. W. Boyle, *Theranostics*, 2012, **2**, 916–966.
36 K. K. Chin, S.-C. Chuang, B. Hernandez, M. Selke, C. S. Foote and M. A. Garcia-Garibay, *J. Phys. Chem. A*, 2006, **110**, 13662–13666.
37 S. Goel, C. G. England, F. Chen and W. Cai, *Adv. Drug Delivery Rev.*, 2017, **113**, 157–176.
38 W. Chen, S. Zhang, Y. Yu, H. Zhang and Q. He, *Adv. Mater.*, 2016, **28**, 8567–8585.
39 A. de Bettencourt-Dias and A. Poloukhtine, *J. Phys. Chem. B*, 2006, **110**, 25638–25645.
40 A. de Bettencourt-Dias, S. Viswanathan and A. Rollett, *J. Am. Chem. Soc.*, 2007, **129**, 15436–15437.
41 S. Hackbarth, S. Pfitzner, L. Guo, J. Ge, P. Wang and B. Röder, *J. Phys. Chem. C*, 2018, **122**, 12071–12076.
42 R. W. Redmond and J. N. Gamlin, *Photochem. Photobiol.*, 1999, **70**, 391–475.
43 K. R. Johnson, M. A. Gracia-Nava and A. de Bettencourt-Dias, *J. Lumin.*, 2020, DOI: 10.1016/j.jlumin.2020.117309.
44 K. R. Johnson, V. C. Lombardi and A. de Bettencourt-Dias, *Chem: Eur. J.*, 2020, DOI: 10.1002/chem.202001568.
45 K. R. Johnson, S. B. Vittardi, M. A. Gracia-Nava, J. J. Rack and A. de Bettencourt-Dias, *Chem. – Eur. J.*, 2020, DOI: 10.1002/chem.202000587.
46 A. de Bettencourt-Dias, S. Viswanathan and K. Ruddy, *Cryst. Growth Des.*, 2005, **5**, 1477–1483.
47 A. de Bettencourt Dias and S. Viswanathan, *Chem. Commun.*, 2004, 1024–1025.
48 S. V. Rocha and N. S. Finney, *J. Org. Chem.*, 2013, **78**, 11255–11261.
49 S. T. Nguyen, A. L. Rheingold, G. S. Tschumper and D. L. Watkins, *Cryst. Growth Des.*, 2016, **16**, 6648–6653.
50 A. Maroń, S. Kula, A. Szlapa-Kula, A. Świtlicka, B. Machura, S. Krompiec, J. G. Małecki, R. Kruszyński, A. Chrobok, E. Schab-Balcerzak, S. Kotowicz, M. Siwy, K. Smolarek, S. Maćkowski, H. Janeczek and M. Libera, *Eur. J. Org. Chem.*, 2017, 2730–2745.
51 S. Encinas, L. Flamigni, F. Barigelletti, E. C. Constable, C. E. Housecroft, E. R. Schofield, E. Figgemeier, D. Fenske, M. Neuburger, J. G. Vos and M. Zehnder, *Chem. – Eur. J.*, 2002, **8**, 137–150.
52 D. C. Young, H. Yang, S. G. Telfer and P. E. Kruger, *Inorg. Chem.*, 2017, **56**, 12224–12231.
53 A. de Bettencourt-Dias and A. Poloukhtine, *J. Phys. Chem. B*, 2006, **110**, 25638–25645.
54 D. T. de Lill and A. de Bettencourt-Dias, *Acta Crystallogr., Sect. E: Struct. Rep. Online*, 2010, **66**, o2124.
55 A. Picot, C. Feuvrie, C. Barsu, F. Malvolti, B. Le Guennic, H. Le Bozec, C. Andraud, L. Toupet and O. Maury, *Tetrahedron*, 2008, **64**, 399–411.
56 A. Tabet, A. Schröder, H. Hartmann, D. Rohde and L. Dunsch, *Org. Lett.*, 2003, **5**, 1817–1820.
57 M. Manuela, M. Raposo, C. Herbivo, V. Hugues, G. Clermont, M. C. R. Castro, A. Comel and M. Blanchard-Desce, *Eur. J. Inorg. Chem.*, 2016, 5263–5273.
58 R. Boch, B. Mehta, T. Connolly, T. Durst, J. T. Arnason, R. W. Redmond and J. C. Scaiano, *J. Photochem. Photobiol., A*, 1996, **93**, 39–47.
59 R. J. Marles, J. B. Hudson, E. A. Graham, C. Soucy-Breau, P. Morand, R. L. Compadre, C. M. Compadre, G. H. N. Towers and J. T. Arnason, *Photochem. Photobiol.*, 1992, **56**, 479–487.
60 G. A. Crosby, R. E. Whan and R. M. Alire, *J. Chem. Phys.*, 1961, **34**, 743–748.
61 J. Zhang, P. D. Badger, S. J. Geib and S. Petoud, *Angew. Chem., Int. Ed.*, 2005, **44**, 2508–2512.
62 D. Kovacs, X. Lu, L. S. Mészáros, M. Ott, J. Andres and K. E. Borbas, *J. Am. Chem. Soc.*, 2017, **139**, 5756–5767.
63 C. Y. Chow, S. V. Eliseeva, E. R. Trivedi, T. N. Nguyen, J. W. Kampf, S. Petoud and V. L. Pecoraro, *J. Am. Chem. Soc.*, 2016, **138**, 5100–5109.
64 Z. Ahmed and K. Iftikhar, *J. Phys. Chem. A*, 2013, **117**, 11183–11201.
65 N. M. Shavaleev, S. J. A. Pope, Z. R. Bell, S. Faulkner and M. D. Ward, *Dalton Trans.*, 2003, 808–814.
66 N. S. Baek, Y. H. Kim, Y. K. Eom, J. H. Oh, H. K. Kim, A. Aebischer, F. Gumy, A.-S. Chauvin and J.-C. G. Bunzli, *Dalton Trans.*, 2010, **39**, 1532–1538.
67 M. Rubio, M. Merchán, E. Ortí and B. O. Roos, *Chem. Phys. Lett.*, 1996, **248**, 321–328.
68 R. S. Becker, J. Seixas de Melo, A. L. Maçanita and F. Elisei, *J. Phys. Chem.*, 1996, **100**, 18683–18695.
69 A. B. Skov, M. A. B. Larsen, M. B. Liisberg, T. Hansen and T. I. Sølling, *Phys. Chem. Chem. Phys.*, 2018, **20**, 13412–13418.
70 D. Fazzi, M. Barbatti and W. Thiel, *Phys. Chem. Chem. Phys.*, 2015, **17**, 7787–7799.
71 T. Schnappinger, M. Marazzi, S. Mai, A. Monari, L. González and R. de Vivie-Riedle, *J. Chem. Theory Comput.*, 2018, **14**, 4530–4540.
72 J. W. G. Bloom and S. E. Wheeler, *J. Chem. Theory Comput.*, 2014, **10**, 3647–3655.
73 J. B. Lin, Y. Jin, S. A. Lopez, N. Druckerman, S. E. Wheeler and K. N. Houk, *J. Chem. Theory Comput.*, 2017, **13**, 5624–5638.